



Hydrothermal synthesis of needle-shaped manganese oxide nanoparticle for superior adsorption of thallium(I): characterization, performance, and mechanism study

Zhichang Ren¹ · Wanlin Wu¹ · Ling Yu² · Yang Yu¹

Received: 29 June 2019 / Accepted: 30 September 2019 / Published online: 19 November 2019
© Springer-Verlag GmbH Germany, part of Springer Nature 2019

Abstract

Thallium as a highly toxic metal element has been listed as one of priority drinking water contaminants. In this study, manganese oxide nanoparticles were synthesized through a simple hydrothermal method and applied for the removal of thallium(I). The adsorbent was composed of numerous needle-like nanorods and had an average volume diameter of 230 nm after heat-drying procedure. The crystal form of adsorbent was determined as α -MnO₂. The adsorbent exhibited a much faster adsorption rate than most of previously reported adsorbent, achieving over 66.4% of equilibrium adsorption capacity in the first 10 min. The adsorption process was found to be highly affected by solution pH and higher than 100 mg/g of adsorption capacity could be obtained in a wide pH range of 6.0–10.0. The isotherm study indicated that the adsorption of Tl(I) on the adsorbent was favorable and governed by a chemisorption process, with the maximum adsorption capacity of 505.5 mg/g at pH 7.0. The adsorption process was confirmed to be thermodynamically spontaneous and endothermic. The presence of Na⁺, K⁺, Mg²⁺, Ca²⁺, and Cu²⁺ cations had certain negative effects on the uptake of Tl(I). Based on the batch experiments and XPS analysis, the deprotonated hydroxyl groups that bonded to manganese atoms worked as the binding sites for the effective removal of Tl(I) ions and no redox reaction occurred during the adsorption process.

Keywords Thallium · Adsorption · Manganese oxide · Hydrothermal synthesis · Mechanism

Introduction

Due to its high toxicity, thallium (Tl) is listed as one of priority drinking water contaminants by the US Environmental Protection Agency (USEPA), with the maximum contaminant level (MCL) of 2 µg/L. The concentration of thallium in natural waters is normally detected at the nanogram per liter level (Cheam et al. 1995), while unacceptable concentration, up to

several milligrams per liter, of thallium in water can be caused by anthropogenic activities, e.g., mining and smelting (Peter and Viraraghavan 2005). It has been reported that the chronic exposure to thallium even at the low concentration can cause a series of serious health issues (Mulkey and Oehme 1993).

In water, thallium exists in two major inorganic forms: thallium(I) and thallium(III). The effective removal of Tl(I) becomes the main challenge because of its higher stability and solubility than Tl(III) (Mulkey and Oehme 1993). Various technologies including chemical precipitation (Davies et al. 2016; Forchheimer and Epple 1951), coagulation/oxidation (Zhang et al. 2013), ion exchange (Horne 1958), biological treatment (Zhang et al. 2017), and adsorption (Chen et al. 2017; Deng et al. 2016) have been reported for the removal of Tl(I) from water. Practically speaking, adsorption is always believed as the most favorable method due to its low cost, simple operation, high efficiency, and wide applicability. Although a large number of adsorbents have been developed for removing Tl(I) from surface water or wastewater (Khavidaki and Aghaie 2013; Liu et al. 2014; Rehman et al. 2013; Wan et al. 2014; Yin et al. 2007; Zhang

Responsible editor: Tito Roberto Cadaval Jr

Electronic supplementary material The online version of this article (<https://doi.org/10.1007/s11356-019-06659-w>) contains supplementary material, which is available to authorized users.

✉ Yang Yu
yuyang@jnu.edu.cn

¹ Guangdong Key Laboratory of Environmental Pollution and Health, School of Environment, Jinan University, Guangzhou 511443, China

² Analysis and Test Center, Guangdong University of Technology, Guangzhou 510006, China

et al. 2018), more efforts are still needed to be devoted on the development of more effective adsorptive materials, especially in terms of the adsorption capacity and rate which are key parameters for the application potential.

Better adsorption performance of thallium removal has been observed for several nano-sized adsorbents owing to their higher specific surface area and/or porosity, stronger affinity towards target contaminants and more abundant functional groups (Huangfu et al. 2014; Zhang et al. 2008). The high affinity of manganese oxide adsorbent towards thallium has been recognized and reported in the literature (Huangfu et al. 2014; Li et al. 2018; Wan et al. 2014). The amorphous hydrous manganese dioxide synthesized through a simultaneous oxidation-precipitation method had the maximum Tl(I) adsorption capacity of 353.6 mg/g at pH 5.0 (Wan et al. 2014). Despite the presence of a magnetic core, the flower-like manganese dioxide-coated magnetic pyrite cinder still performed a maximum Tl(I) adsorption capacity of 320 mg/g at pH 12.0. The hydrothermal synthetic route is considered as the most attracting method for the preparation of nano-sized materials. The formed particles from hydrothermal reaction generally have smaller particle size, more uniform size distribution, and better dispersibility in water (Liu et al. 2014; Yu et al. 2016). As reported by Liu et al. (2014), titanate nanotubes synthesized through a simple hydrothermal method exhibited a maximum adsorption capacity as high as 709.2 mg/g towards Tl(I) at pH 5.0. To our knowledge, the hydrothermally synthesized manganese oxide nanoparticle has not yet been reported in the literature for the effective removal of Tl(I) ions from water.

In this study, a new manganese oxide nano-sized adsorbent with strong affinity and rapid adsorption rate towards Tl(I) ions was prepared by a one-step hydrothermal method. The physiochemical properties of the adsorbent were investigated by scanning electron microscope (SEM), X-ray diffraction (XRD), transmission electron microscopy (TEM), dynamic light scattering (DLS), and X-ray photoelectron spectroscopy (XPS). The adsorption performance of the adsorbent on the removal of Tl(I) was studied by a series of batch experiments and the adsorption mechanism was proposed as well. The findings from this study would be beneficial for promoting the development of more effective and economical treatment techniques for thallium decontamination.

Materials and methods

Materials

Potassium permanganate (KMnO_4), sulfuric acid (H_2SO_4), sodium hydroxide (NaOH), nitric acid (HNO_3), thallium(I) nitrate (TlNO_3), sodium chloride (NaCl), potassium chloride (KCl), magnesium chloride hexahydrate ($\text{MgCl}_2 \cdot 6\text{H}_2\text{O}$),

calcium chloride dihydrate ($\text{CaCl}_2 \cdot 2\text{H}_2\text{O}$), and copper chloride dihydrate ($\text{CuCl}_2 \cdot 2\text{H}_2\text{O}$) were purchased from Aladdin Chemicals (Shanghai, China). All chemicals used in this study were of analytical grade without further purification.

Adsorbent preparation

The manganese oxide nanoparticles were synthesized via a one-step hydrothermal method. In brief, 0.2 g of KMnO_4 was dissolved into 60 mL of deionized (DI) water under ultrasonication. Then, 2.0 mL of 5% H_2SO_4 was added into the solution. After agitation for 30 min, the solution was transferred into a 100-mL Teflon-line autoclave at 160 °C for 8 h. The formed particles were collected, washed by DI for several times, and dried in oven at 60 °C.

Characterization

The surface morphology of manganese oxide nanoparticles was investigated by SEM (ZEISS EVO18, Germany). The crystal structure of the adsorbent was visualized through XRD (Bruker D2 Phaser, Germany) using copper $\text{K}\alpha$ radiation with 2θ scan range of 10–80° and a step size of 0.02°. TEM was performed on the JEOL 2100F equipment. The zeta potential and size distribution of the particles were determined by dynamic light scattering (Zetasize nano ZSE, Malvern, UK). The surface element composition and oxidation states of key elements were analyzed by XPS (Kratos XPS system-Axis His-165 Ultra, Shimadzu, Japan) at 15 kV, 10 mA, and a base pressure of 3×10^{-8} Torr in the chamber with an Al $\text{K}\alpha$ X-ray source (150 W). All XPS results in binding energy forms were fitted using a nonlinear least squares curve fitting program (XPSPEARK Software, Version 4.1).

Batch experiments

All the batch adsorption experiments were carried out on a rotary shaker at the room temperature (25 ± 1 °C). For the adsorption kinetics study, 1 L of Tl(I) solution with the initial concentration of 12.5 mg/L was prepared by dissolving Tl(I) stock solution into DI water. The solution pH was adjusted to 7.0 and maintained throughout the adsorption by adding a certain amount of HNO_3 or NaOH . After adding 0.1 g of the adsorbent, samples were taken at different time intervals and filtered through 0.45 μm PES membranes. For the pH effect study, the pH of 12.5 mg/L Tl(I) solutions was adjusted to different values in the range of 3.0–10.0. The solution pH was controlled during the experiment and the adsorbent dosage was 0.1 g/L. After agitation for 24 h, samples were taken for concentration measurement. In order to evaluate the stability of adsorbent under different solution pH, the concentration of manganese ions in solution after the adsorption was also measured. For the isotherm study, the initial concentrations of

Tl(I) solutions were varied from 1 to 50 mg/L. The solution pH was controlled at 7.0. Samples were taken after shaking for 24 h. In order to evaluate the influence of co-existing cations in the uptake of Tl(I), different amounts of Na⁺, K⁺, Mg²⁺, Ca²⁺, and Cu²⁺ were respectively added into 12.5 mg/L Tl(I) solutions. The solution pH was controlled at 5.0 during the adsorption process. Other procedures were the same as those in aforementioned experiments. Four-cycle adsorption and desorption experiments were carried out to evaluate the regeneration ability of the adsorbent. 0.1 g of virgin adsorbent was added into 1 L of 12.5 mg/L Tl(I) solution under stirring and the solution pH was controlled at 7.0. After the adsorption, the spent adsorbent was regenerated using 0.1 M HNO₃ solution under stirring for 3 h. The regenerated adsorbent was washed by DI water and then used for the next cycle of adsorption experiment.

The concentration of Tl(I) in samples was determined using an inductively coupled plasma mass spectrometry (ICP-MS). The adsorption capacity of Tl(I) was calculated as follows:

$$q_t = \frac{(C_0 - C_t)V}{m} \quad (1)$$

where q_t is the adsorbed amount of Tl(I) at time t (mg/g), C_0 and C_t are the concentrations of Tl(I) at initial and time t , respectively (mg/L), V is the solution volume (L), and m is the mass of the adsorbent in solution (g).

Results and discussion

Characterization of the adsorbent

As shown in Fig. 1a, the adsorbent is aggregated by needle-like nanorods after the heat-drying procedure, resulting in a high surface area and porous structure. This should be beneficial for the diffusion of Tl(I) to all the adsorptive sites on the

adsorbent. The hydrothermally synthesized adsorbent was directly collected by vacuum filtration, washed by DI water for several times, and then homogeneously dispersed in water for the particle size distribution analysis. As shown in Fig. 1b, the particle size of adsorbent is in the range of 100–1000 nm, and the mean volume diameter is approximately 230 nm.

XRD was employed for the analysis of the crystal structure of adsorbent. Figure 2a shows that characteristic peaks at 18.4°, 29.0°, 37.7°, 50.4°, 56.8°, 60.5°, 65.5°, 69.7°, and 72.6° can be observed in the XRD pattern of adsorbent, typical of pure α -MnO₂ phase (PDF No. 44-0141). The surface element composition of adsorbent was determined by XPS. As seen from Fig. 2b, the characteristic peaks of manganese and oxygen elements including Mn 3p, Mn 2p, Mn 2s, O 1s, and O KL1 can be detected in the wide scan spectrum of the virgin adsorbent.

The low-magnification TEM image shows manganese oxide nanoparticles have a long needle-like shape (Fig. 3a). It is further confirmed from the TEM image as shown in Fig. 3b that the crystals are layer structured.

Adsorption kinetics

As well known, the adsorption rate is a key parameter for the practical application of adsorbents. As demonstrated in Fig. 4a, approximately 66.4% of equilibrium Tl(I) adsorption capacity can occur within the initial 10 min. This means that a shorter hydraulic retention time (HRT) is required when the prepared adsorbent is applied for treating thallium-contaminated water. The adsorption equilibrium can be obtained in 10 h.

To better understand the adsorption process, the pseudo-first-order, pseudo-second-order, and intraparticle diffusion models were employed for fitting the experimental data. The mathematical equations of models are expressed as follows:

$$\ln(q_e - q_t) = \ln q_e - K_1 t \quad (2)$$

Fig. 1 SEM image (a) and particle size distribution (b) of manganese oxide nanoparticle

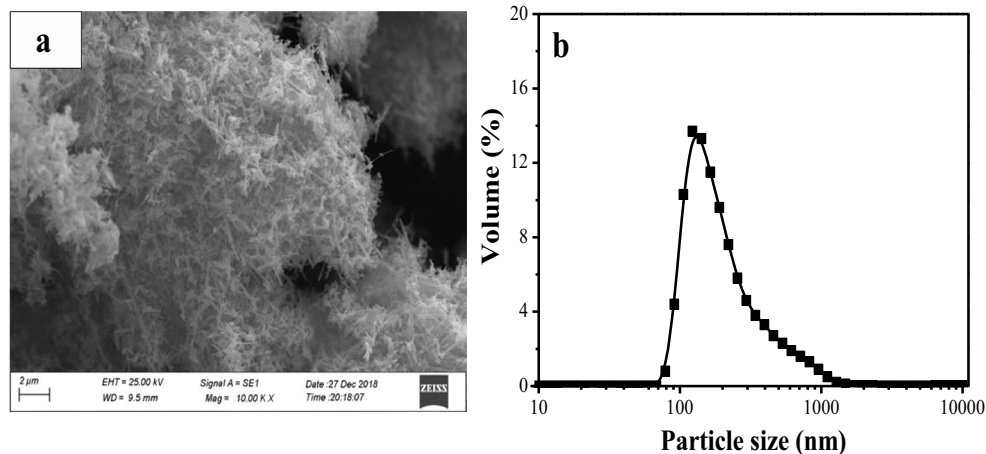
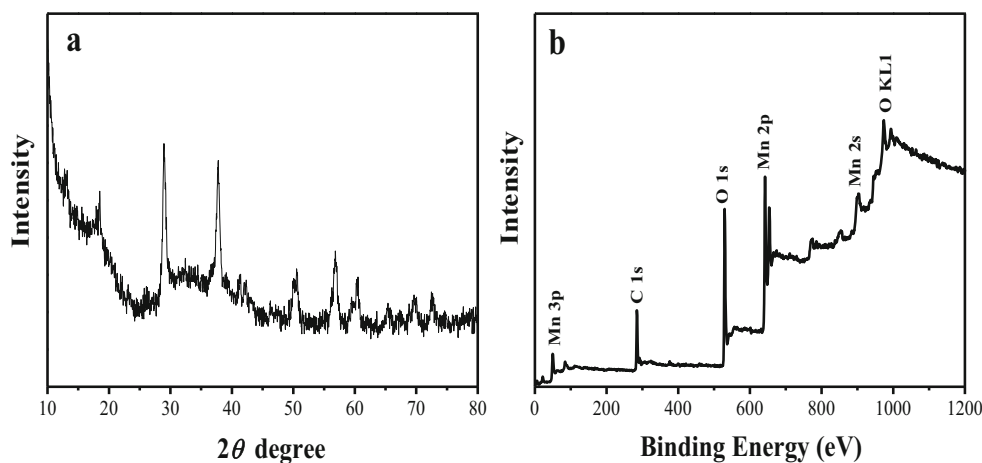


Fig. 2 XRD pattern (a) and wide scan XPS spectrum (b) of manganese oxide nanoparticle



$$t/q_t = 1/(K_2q_e^2) + t/q_e \tag{3}$$

$$q_t = K_{id}t^{1/2} + \alpha \tag{4}$$

where q_e and q_t are adsorption capacities of Tl(I) at equilibrium and time t (mg/g), respectively. K_1 (h^{-1}), K_2 ($g\ mg^{-1}\ h^{-1}$), and K_{id} ($mg\ g^{-1}\ h^{-1/2}$) are the related rate constants of the pseudo-first-order, pseudo-second-order, and intraparticle diffusion models, respectively. α (mg/g) represents to effect of the boundary layer, and t is the time (h).

The rate constants and correlation coefficients from models are illustrated in Table 1. The pseudo-second-order model seems to have better fitting of experimental data than the pseudo-first-order model according to correlation coefficients, suggesting that the chemisorption process is mainly involved in the uptake of Tl(I). A comparison of previously reported adsorbents for Tl(I) removal is summarized in Table 2. The manganese oxide nanoparticles show a more excellent performance in terms of the adsorption rate (K_1) and adsorption capacity in 30 min than most of adsorbents. This indicates that the prepared adsorbent has great application potential for effectively and economically treating thallium-contaminated water.

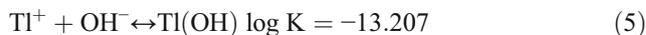
The intraparticle diffusion model was used to investigate the adsorption rate limiting step of the Tl(I) adsorption process. It can be seen from Fig. 4b and Table 1 that two linear stages are involved in the adsorption process. The adsorption rate of the first linear stage corresponding to the intraparticle

diffusion is determined as $23.30\ mg\ g^{-1}\ h^{-1/2}$. The value of α_1 is found to be as high as $61.7\ mg/g$ (equal to 59.5% of equilibrium adsorption capacity), suggesting that the adsorption rate of Tl(I) is highly affected by boundary layer effect or external diffusion process. Increasing agitation intensity can effectively reduce the thickness of boundary layer and accelerate the diffusion of adsorbate through the liquid film (Kyzas et al. 2012). The second linear stage represents the equilibrium process of which rate constant drops significantly due to the reduction of Tl(I) concentration in solution.

Influence of solution pH

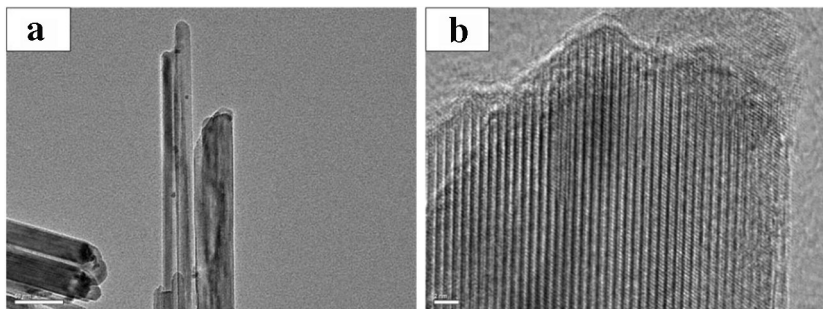
As chemical properties of adsorbent and adsorbate can be highly affected by solution pH, it is important to evaluate the influence of solution pH on the uptake of Tl(I). As shown in Fig. 5a, the basic condition is more favorable for the adsorption process and the optimal adsorption takes place in the pH range of 6.0–10.0.

The dissociation constant for Tl(I) hydroxyl complexes used in MINEQL+4.5 Software is expressed as below:



Based on Eq. (5), the dominant species of Tl(I) are Tl^+ ions in the tested pH range of 3.0–10.0. The zeta potential of adsorbent under different solution pH was measured in this

Fig. 3 TEM images of needle-shaped manganese oxide nanoparticle



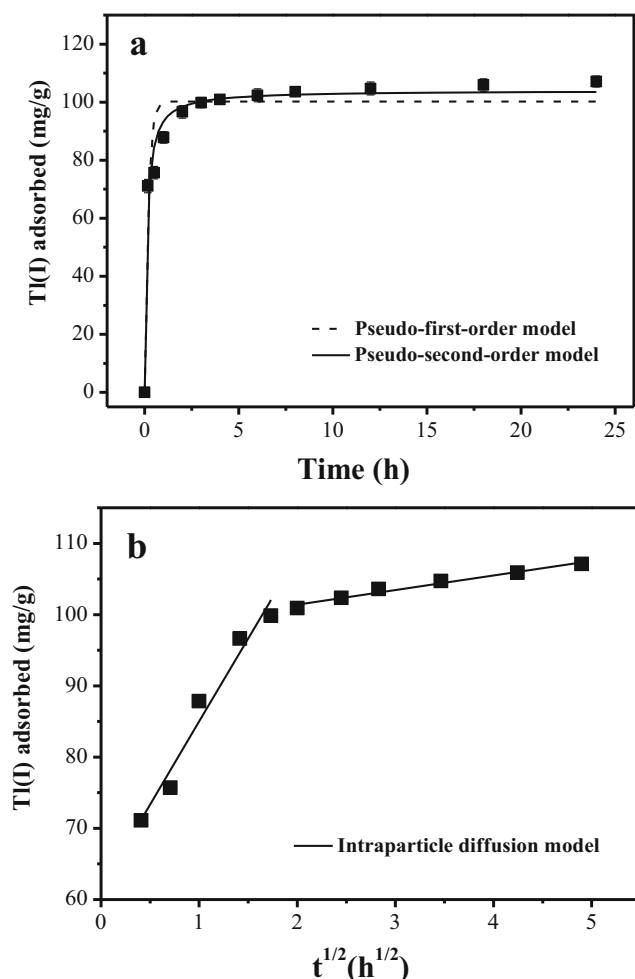


Fig. 4 Kinetics of Tl(I) adsorption on manganese oxide nanoparticle. Fitted by the pseudo-first-order and pseudo-second-order models (a) and fitted by the intraparticle diffusion model (b). $[Tl(I)]_0 = 12.5$ mg/L; adsorbent dosage = 0.1 g/L; $p = 7.0$; $T = 25 \pm 1$ °C

study. The isoelectric point (IEP, solution pH at which the zeta potential equals zero) is widely applied for characterizing net charge of the adsorbent surface. At the pH value of IEP, the adsorbent surface is considered to be neutrally charged due to the equilibrium of protonation and deprotonation of surface functional groups on the adsorbent. The value of IEP of adsorbent is determined as 5.6 as shown in Fig. 5b. Therefore, a positive surface charge would be formed on the adsorbent at pH below 5.6, leading to the enhancement of electrostatic repulsion between the adsorbent and Tl(I) ions. The adsorption capacity of Tl(I) is obviously depressed at pH below 5.0.

In contrast, the negatively charged adsorbent surface at pH above 5.6 would be beneficial for the diffusion and adsorption of Tl(I) towards the adsorptive sites on the adsorbent due to the electrostatic attraction between the adsorbent and Tl(I). Noted that the adsorption capacity is above 100 mg/g in a wide pH range of 6.0–10.0 because of its high affinity towards Tl(I) ions. The adsorbent can be therefore potentially applied for the wastewater treatment where pH may vary a lot depending on the industrial types.

The stability of adsorbent was evaluated through measuring the concentration of manganese ions in the solution after the adsorption. As seen from Fig. 5a, more obvious dissolution of the adsorbent can be observed under acidic condition. However, even at pH 3.0, the dissolved manganese mass was only approximately 1.15% of the virgin adsorbent, indicating that the adsorbent can maintain a good stability in the tested pH range.

Adsorption isotherm

The adsorption isotherm of Tl(I) on the adsorbent was studied at pH 7.0 and the experimental data together with the fitting results from the Langmuir and Freundlich models are shown in Fig. 6. The mathematical equations are given as follows:

$$q_e = \frac{q_{\max} b C_e}{1 + b C_e} \quad (6)$$

$$q_e = k_f C_e^{1/n} \quad (7)$$

where q_e (mg/g) and C_e (mg/L) are the adsorbed amount of Tl(I) at equilibrium and the relative equilibrium concentration of Tl(I) in solution, respectively, q_{\max} (mg/g) is the maximum adsorption capacity, b is the Langmuir isotherm constant relating to the strength of adsorption (L/mg), k_f is a constant for relative adsorption capacity ($\text{mg}^{(1-1/n)}\text{L}^{1/n}/\text{g}$), and n is an affinity constant.

According to the constants illustrated in Table 3, the Langmuir isotherm model seems to be more suitable for simulating the experimental data than the Freundlich isotherm model. The maximum adsorption capacity of the adsorbent is 505.5 mg/g at pH 7.0, much higher than most of previously reported adsorbents (Table 2). The favorability of the adsorption process is further evaluated by the dimensionless constant separation factor (R_L) as the expression below:

$$R_L = \frac{1}{1 + b C_0} \quad (8)$$

Table 1 Kinetics parameters for Tl(I) adsorption on manganese oxide nanoparticle

Pseudo-first order			Pseudo-second order			Intraparticle diffusion					
q_e (mg/g)	K_1 (h^{-1})	r^2	q_e (mg/g)	K_2 ($\text{g mg}^{-1} \text{h}^{-1}$)	r^2	$K_{id,1}$ ($\text{mg g}^{-1} \text{h}^{-1/2}$)	α_1 (mg/g)	r^2	$K_{id,2}$ ($\text{mg g}^{-1} \text{h}^{-1/2}$)	α_2 (mg/g)	r^2
99.59	5.99	0.92	103.7	0.089	0.98	23.30	61.7	0.95	2.043	97.3	0.96

Table 2 Comparison of adsorption rate and capacity of different adsorbents

Adsorbent	pH	Adsorption rate ^a		q_{max} (mg/g) ^c	Reference
		K_1 (h ⁻¹)	$q_{0.5 h}$ (mg/g) ^b		
Treated sawdust	7.0	--	--	13.2	Memon et al. (2008)
Polyacrylamide-zeolite	5.0	--	--	378.1	Şenol and Ulusoy (2010)
Polyacrylamide-bentonite	5.0	--	--	73.6	Şenol and Ulusoy (2010)
Titanium peroxide	7.0	94.05 (18.5)	~ 85 (18.5)	356	Zhang et al. (2017)
Titanate nanotubes	5.0	0.015 (50.0)	~ 251 (50.0)	709.2	Liu et al. (2014)
Modified fungal biomass	5.0	1.27 (10.0)	~ 2.2 (10.0)	159.7	Peter and Viraraghavan (2008)
Multiwalled carbon nanotube	7.0	--	~ 2.2 (0.1)	0.42	Pu et al. (2013)
Prussian blue-alginate capsules	4.0	1.02 (20)	~ 25 (20)	103.0	Vincent et al. (2014)
Manganese oxide nanoparticle	7.0	5.99 (12.5)	75.7 (12.5)	505.5	This study

^a Initial Tl(I) concentration (mg/L) is listed in parentheses

^b $q_{0.5 h}$ refers to the adsorption capacity within 0.5 h

^c q_{max} refers to the maximum adsorption capacity given by the Langmuir isotherm

where R_L is the dimensionless constant separation factor relating to the type of the Langmuir isotherm (Hall et al. 1966), and C_0 (mg/L) is the initial concentration of Tl(I) in solution.

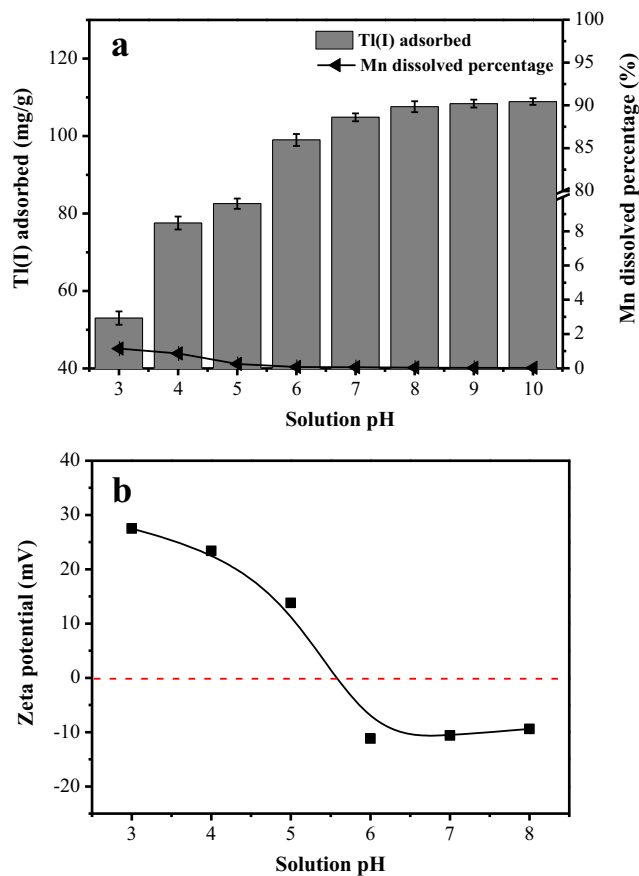


Fig. 5 Effect of solution pH on Tl(I) adsorption and adsorbent stability (a) and zeta potential of manganese oxide nanoparticle (b). [Tl(I)]₀ = 12.5 mg/L; adsorbent dosage = 0.1 g/L; $T = 25 \pm 1$ °C

The adsorption would be irreversible and linear when R_L is respectively equal to 0 and 1, favorable when $0 < R_L < 1$, and unfavorable as $R_L > 1$ (Memon et al. 2008). The values of R_L calculated in this study are varied between 0.07 and 0.77, demonstrating that Tl(I) can be favorably adsorbed on the adsorbent.

The Dubinin-Radushkevich model was also employed for simulating the isotherm experimental data. The equation is described as below:

$$\ln q_e = \ln q_{max} - \beta \varepsilon^2 \tag{9}$$

$$\varepsilon = RT \ln(1 + 1/C_e) \tag{10}$$

$$E = (2\beta)^{-0.5} \tag{11}$$

where β (mol²/J²) is the constant related to mean adsorption

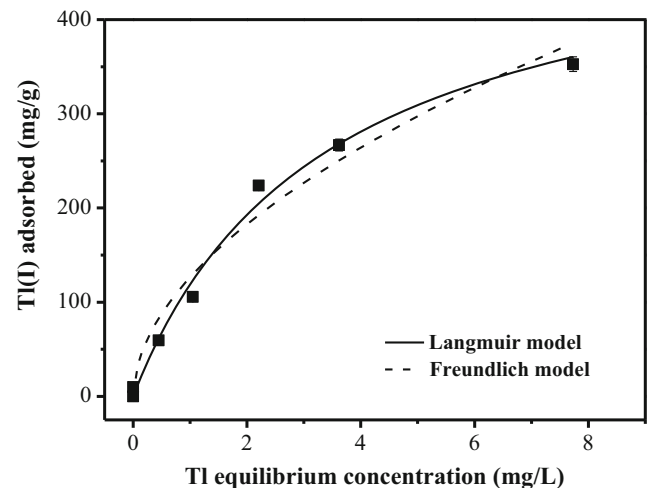


Fig. 6 Adsorption isotherm of Tl(I) on manganese oxide nanoparticle at pH 7.0. Adsorbent dosage = 0.1 g/L; $T = 25 \pm 1$ °C

Table 3 Isotherm constants for the adsorption of Tl(I)

Langmuir isotherm			Freundlich isotherm			Dubinin-Radushkevich isotherm		
q_{max} (mg/g)	b (L/mg)	r^2	k_f (mg ^(1-1/n) L ^{1/n} /g)	$1/n$	r^2	E (kJ/mol)	β (mol ² /kJ ²)	r^2
505.5	0.309	0.98	126.0	0.525	0.96	8.452	0.007	0.93

energy, ε is the Polanyi potential related to the equilibrium concentration, R (8.314 J/(mol·K)) is molar gas constant, T (K) is the thermodynamic temperature, and E (J/mol) is the mean free energy of the adsorption process.

As shown in Fig. S1, the linear Dubinin-Radushkevich isotherm model was constructed via the plot of $\ln q_e$ versus ε^2 . It can be seen from Table 3 that the values of E and β calculated from the slope are 8.452 kJ/mol and 0.007 mol²/kJ², respectively. This confirms that the adsorption of Tl(I) ions on the adsorbent surface is dominated by a chemisorption process (Ali et al. 2014; Lu et al. 2014; Şakir et al. 2018).

The thermodynamic studies were conducted at 298, 308, 318, and 328 K at pH 7.0. The values of corresponding parameters such as Gibbs free energy change (ΔG^0), enthalpy change (ΔH^0), and entropy change (ΔS^0) were calculated according to the following equations:

$$K = \frac{C_{ad}}{C_{eq}} \quad (12)$$

$$\Delta G^0 = -RT \ln K \quad (13)$$

$$\Delta G^0 = \Delta H^0 - T \Delta S^0 \quad (14)$$

$$\ln K = \frac{\Delta S^0}{R} - \frac{\Delta H^0}{RT} \quad (15)$$

where K is the adsorption equilibrium constant, C_{ad} (mg/L) and C_{eq} (mg/L) are the Tl(I) concentrations on the adsorbent and solution, respectively.

As shown in Fig. S2 and Table 4, the values of free energy change under different temperature are negative and decrease with the increase of reaction temperature, suggesting that the adsorption process is thermodynamically spontaneous and become more feasible at high temperature. Similar to other studies (Zhang et al. 2008), the ΔH^0 and ΔS^0 values are found to be positive during the Tl(I) adsorption. Since the Tl(I) ions are hydrated in solution, previously bonded water molecules need to be released prior to the adsorption of Tl(I) ions on the

Table 4 Thermodynamic parameters for Tl(I) adsorption

T (K)	Ln K	ΔG^0 (kJ/mol)	ΔH^0 (kJ/mol)	ΔS^0 (kJ/mol·K)
298	1.37	-3.39	22.04	0.085
308	1.57	-4.03		
318	1.88	-4.97		
328	2.26	-6.20		

adsorbent surface, leading to the endothermic nature of the adsorption process.

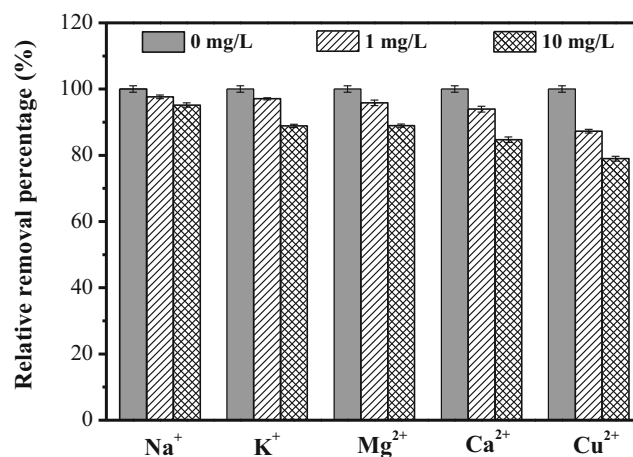
Adsorption selectivity

The adsorption selectivity of Tl(I) on the adsorbent was studied by respectively adding a certain amount of Na⁺, K⁺, Mg²⁺, Ca²⁺, and Cu²⁺ into Tl(I) solutions at pH 5.0. As shown in Fig. 7, the presence of aforementioned cations can cause some interference in the uptake of Tl(I). It is worthwhile to note that K⁺ ions are found to have more significant influence on the adsorption than Na⁺ ions. When 10 mg/L K⁺ ions are present in water, the uptake of Tl(I) decreases by 11.2%. The more notable competitive effect of K⁺ ions might be due to its similar ionic radii with Tl(I) ions (Galván-Arzate and Santamaría 1998). The effect of divalent cations (e.g., Mg²⁺, Ca²⁺, and Cu²⁺) on the adsorption follows the order of Cu²⁺ > Ca²⁺ > Mg²⁺. The higher electronegativity of Mg²⁺, Ca²⁺, and Cu²⁺ than Tl(I) ions would cause stronger competition towards the active sites on the adsorbent (Kinraide and Yermiyahu 2007).

The regeneration performance of the adsorbent was evaluated by using 0.1 M HNO₃ as the regenerant and the results are shown in Fig. 8. It can be seen that the adsorption capacity can be respectively restored to 87.6% and 54.3% of original adsorption capacity after the first and fourth regeneration cycles.

Adsorption mechanism

The XPS analysis was applied for better understanding of the chemical interaction between the adsorbent and Tl(I). As seen

**Fig. 7** Adsorption selectivity of Tl(I) on manganese oxide nanoparticle. [Tl(I)]₀ = 12.5 mg/L; adsorbent dosage = 0.1 g/L; T = 25 ± 1 °C; pH = 5.0

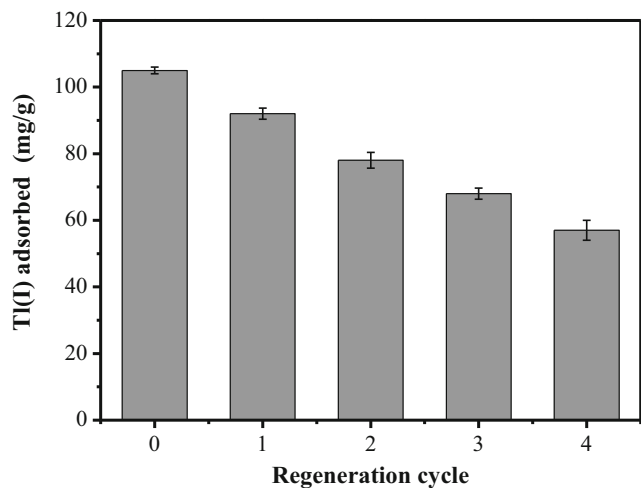


Fig. 8 Regeneration studies of manganese oxide nanoparticle. [Tl(I)]₀ = 12.5 mg/L; adsorbent dosage = 0.1 g/L; T = 25 ± 1 °C; pH = 7.0

from Fig. 9a, the appearance of new peaks assigned to Tl 4f and Tl 4d on the Tl-loaded adsorbent indicates that Tl(I) has been successfully adsorbed on the adsorbent.

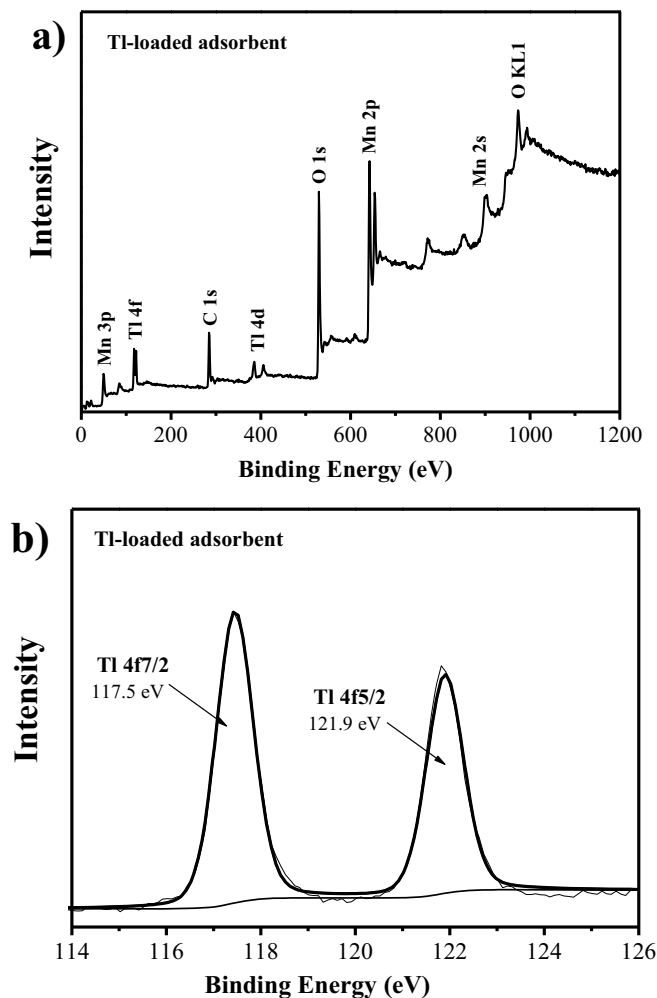
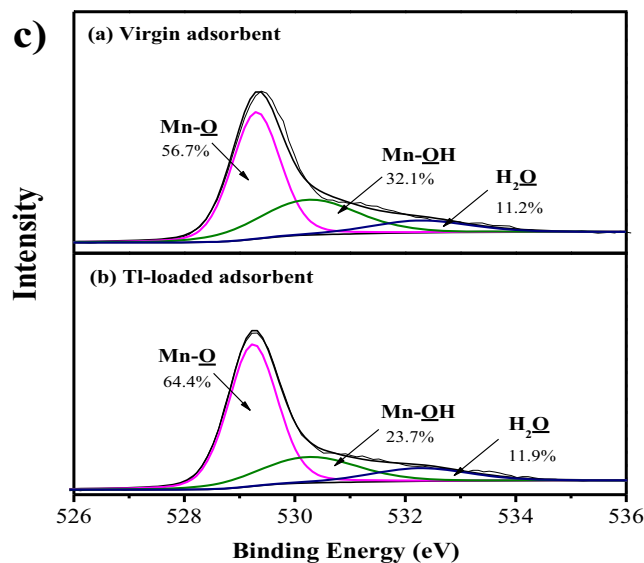


Fig. 9 Wide scan (a), Tl 4f (b), and O 1s (c) XPS spectra of virgin and Tl-loaded adsorbents

As shown in Fig. 9b, the high-resolution XPS spectrum of thallium element on the adsorbent after the adsorption consists of two component peaks corresponding to Tl 4f_{7/2} and Tl 4f_{5/2}, with the binding energies of 117.5 and 121.9 eV, respectively. The oxidation state of the adsorbed thallium ions is still +I and there is no oxidation of Tl(I) occurred on the adsorbent surface (Wan et al. 2014; Zhang et al. 2018).

Since the functional groups on the adsorbent may play a key role in the uptake of Tl(I), the composition of oxygen-containing groups was analyzed by the O 1s high-resolution XPS spectra of the adsorbents before and after the adsorption and the results are shown in Fig. 9c. Specifically, the O 1s spectra can be decomposed into three component peaks, of which peaks at the binding energies of 529.2, 530.2, and 532.3 eV can be attributed to the manganese–oxygen bond (Mn–O), hydroxyl groups bonded to manganese atoms (Mn–OH), and adsorbed water (H₂O), respectively. After the adsorption, the contents of Mn–O and adsorbed H₂O increase from 56.7 to 64.4% and 11.2 to 11.9%, respectively. Meanwhile, the relative content of Mn–OH decreases from 32.1 to 23.7%. This finding confirms that the hydroxyl groups



bonded to manganese atoms are involved in the adsorption process of Tl(I).

Based on the aforementioned results, the abundant hydroxyl groups bonded to manganese atoms are highly involved in the uptake of Tl(I) ions. Under different solution pH, the surface charge of the adsorbent would be varied due to the protonation or deprotonation of hydroxyl groups, which can obviously affect the diffusion of Tl(I) ions towards the adsorptive active sites and the adsorption process. During the adsorption, Tl(I) ions can be rapidly adsorbed on the adsorbent surface through the formation of the linkages of Mn–O–Tl.

Conclusions

The hydrothermally synthesized manganese oxide nanoparticles with a loose structure were aggregated by numerous needle-like nanorods. TEM images showed that the crystals were observed to be layer structured. The average volume diameter of adsorbent was 230 nm. The isotherm study demonstrated that maximum adsorption capacity of the adsorbent could reach 505.5 mg/g at pH 7.0, much higher than most of previously reported adsorbents. A rapid adsorption rate was observed in adsorption kinetics study in which approximately 66.4% of equilibrium Tl(I) adsorption capacity could be achieved within the initial 10 min. The adsorbent showed an excellent adsorption performance in a wide pH range of 6.0–10.0. The uptake of Tl(I) on the adsorbent was found to be thermodynamically spontaneous and endothermic. The presence of co-existing cations could cause some negative impact on the adsorption process. The hydroxyl groups bonded to manganese atoms played a key role in the adsorption process. The prepared adsorbent with extremely high adsorption capacity and rate would become a potential adsorptive material for the removal of thallium from water.

Funding information This research was supported by Natural Science Foundation of Guangdong Province (Grant No. 2018A0303130148) and Guangzhou Science and Technology Program (Grant No. 201704020138).

References

- Ali I, Al-Othman ZA, Alwarthan A, Asim M, Khan TA (2014) Removal of arsenic species from water by batch and column operations on bagasse fly ash. *Environ Sci Pollut Res* 21:3218–3229
- Cheam V, Lechner J, Desrosiers R, Sekerka I, Lawson G, Mudroch A (1995) Dissolved and total thallium in Great Lakes waters. *J Great Lakes Res* 21:384–394
- Chen M, Wu P, Yu L, Liu S, Ruan B, Hu H, Zhu N, Lin Z (2017) FeOOH-loaded MnO₂ nano-composite: an efficient emergency material for thallium pollution incident. *J Environ Manag* 192:31–38
- Davies M, Figueroa L, Wildeman T, Bucknam C (2016) The oxidative precipitation of thallium at alkaline pH for treatment of mining influenced water. *Mine Water Environ* 35:77–85
- Deng HM, Chen YH, Wu HH, Liu T, Wang YL, Wu GY, Ye HP (2016) Adsorption of Tl(I) on Na–montmorillonite and kaolinite from aqueous solutions. *Environ Earth Sci* 75:752
- Forchheimer OL, Epple RP (1951) Precipitation of thallium(I) from perchloric acid solutions. *Anal Chem* 23:1445–1447
- Galván-Arzate S, Santamaría A (1998) Thallium toxicity. *Toxicol Lett* 99:1–13
- Hall KR, Eagleton LC, Acrivos A, Vermeulen T (1966) Pore- and solid-diffusion kinetics in fixed-bed adsorption under constant-pattern conditions. *Ind Eng Chem Fundam* 5:587–594
- Horne RA (1958) The ion-exchange resin adsorption of thallium(I) and (III). *J Inorg Nucl Chem* 6:338–343
- Huangfu X, Jiang J, Lu X, Wang Y, Liu Y, Pang SY, Cheng H, Zhang X, Ma J (2014) Adsorption and oxidation of thallium(I) by a nanosized manganese dioxide. *Water Air Soil Pollut* 226:2272
- Khavidaki HD, Aghaie H (2013) Adsorption of thallium(I) ions using Eucalyptus leaves powder. *Clean Soil Air Water* 41:673–679
- Kinraide TB, Yermiyahu U (2007) A scale of metal ion binding strengths correlating with ionic charge, Pauling electronegativity, toxicity, and other physiological effects. *J Inorg Biochem* 101:1201–1213
- Kyzas GZ, Lazaridis NK, Mitropoulos AC (2012) Removal of dyes from aqueous solutions with untreated coffee residues as potential low-cost adsorbents: equilibrium, reuse and thermodynamic approach. *Chem Eng J* 189–190:148–159
- Li H, Li X, Xiao T, Chen Y, Long J, Zhang G, Zhang P, Li C, Zhuang L, Li K (2018) Efficient removal of thallium(I) from wastewater using flower-like manganese dioxide coated magnetic pyrite cinder. *Chem Eng J* 353:867–877
- Liu W, Zhang P, Borthwick AGL, Chen H, Ni J (2014) Adsorption mechanisms of thallium(I) and thallium(III) by titanate nanotubes: ion-exchange and co-precipitation. *J Colloid Interface Sci* 423:67–75
- Lu DL, Ji F, Wang W, Yuan SJ, Hu ZH, Chen TH (2014) Adsorption and photocatalytic decomposition of roxarsone by TiO₂ and its mechanism. *Environ Sci Pollut Res* 21:8025–8035
- Memon SQ, Memon N, Solangi AR, Memon JUR (2008) Sawdust: a green and economical sorbent for thallium removal. *Chem Eng J* 140:235–240
- Mulkey JP, Oehme FW (1993) A review of thallium toxicity. *Vet Hum Toxicol* 35:445–453
- Peter ALJ, Viraraghavan T (2005) Thallium: a review of public health and environmental concerns. *Environ Int* 31:493–501
- Peter ALJ, Viraraghavan T (2008) Removal of thallium from aqueous solutions by modified *Aspergillus niger* biomass. *Bioresour Technol* 99:618–625
- Pu Y, Yang X, Hong Z, Wang D, Yu S, Jie H (2013) Adsorption and desorption of thallium(I) on multiwalled carbon nanotubes. *Chem Eng J* 219:403–410
- Rehman SU, Ullah N, Kamali AR, Ali K, Yerlikaya C, Rehman HU (2013) Study of thallium(III) adsorption onto multiwall carbon nanotubes. *Carbon* 55:375–375
- Şakir Y, Ecer Ü, Şahan T (2018) Modelling and optimization of As(III) adsorption onto thiol-functionalized bentonite from aqueous solutions using response surface methodology approach. *ChemistrySelect* 3:9326–9335
- Şenol ZM, Ulusoy U (2010) Thallium adsorption onto polyacrylamide-aluminosilicate composites: a Tl isotope tracer study. *Chem Eng J* 162:97–105
- Vincent T, Taulemesse JM, Dauvergne A, Chanut T, Testa F, Guibal E (2014) Thallium(I) sorption using Prussian blue immobilized in alginate capsules. *Carbohydr Polym* 99:517–526

- Wan S, Ma M, Lv L, Qian L, Xu S, Xue Y, Ma Z (2014) Selective capture of thallium(I) ion from aqueous solutions by amorphous hydrous manganese dioxide. *Chem Eng J* 239:200–206
- Yin CY, Aroua MK, Daud WMAW (2007) Impregnation of palm shell activated carbon with polyethyleneimine and its effects on Cd^{2+} adsorption. *Colloids Surf A Physicochem Eng Asp* 307:128–136
- Yu Y, Yu L, Sun M, Chen JP (2016) Facile synthesis of highly active hydrated yttrium oxide towards arsenate adsorption. *J Colloid Interface Sci* 474:216–222
- Zhang L, Huang T, Zhang M, Guo X, Yuan Z (2008) Studies on the capability and behavior of adsorption of thallium on nano- Al_2O_3 . *J Hazard Mater* 157:352–357
- Zhang H, Chen D, Cai S, Guoqing TU, Luo D, Chen Y (2013) Research on treating thallium by enhanced coagulation oxidation process. *Agric Sci Technol* 14:1322–1324
- Zhang H, Li M, Yang Z, Sun Y, Yan J, Chen D, Chen Y (2017) Isolation of a non-traditional sulfate reducing-bacteria *Citrobacter freundii* sp. and bioremoval of thallium and sulfate. *Ecol Eng* 102:397–403
- Zhang G, Fang F, Li X, Qi J, Chen Y (2018) Superior adsorption of thallium(I) on titanium peroxide: performance and mechanism. *Chem Eng J* 331:471–479

Publisher's note Springer Nature remains neutral with regard to jurisdictional claims in published maps and institutional affiliations.